A Combining FPE and Additional Test Vectors Hybrid Strategy for IPMSM Sensorless Control

Xin Luo, Qipeng Tang, *Student Member, IEEE*, Anwen Shen, Hanlin Shen, and Jinbang Xu

***Abstract*—This paper proposes a hybrid strategy by combining fundamental pulsewidth modulation excitation (FPE) and additional test vectors, which is used in interior permanent-magnet synchronous motor (IPMSM) sensorless control. In contrast to the typical indirect flux detection by on-line reactance measurement-based methodology where the rotor position is calculated and updated in every three successive pulsewidth modulation (PWM) cycles, the proposed hybrid strategy can achieve the one-cycle acquisition of the rotor position by utilizing both response currents of FPE and additional test vectors, which makes the proposed strategy more robust and suitable in higher speed or load sudden change conditions. Meanwhile, a new PWM scheme for four-space-vector PWM (FSVPWM) is presented, which sharply simplifies the implementation process. Furthermore, for the case that the amplitude of the object fundamental voltage is so small that it cannot satisfy minimum time demand for the slopes of response currents sampling, a compensation technique is presented. In addition, the multiple-point current sampling (MPCS) technology and linear least square fitting method are used to decrease the current sampling disturbance, which improves obviously the accuracy of position estimation. Finally, the experimental results confirm that the proposed strategy can obtain the rotor position accurately and simply.**

***Index Terms*—Additional test vectors, four-space-vector pulsewidth modulation (FSVPWM), fundamental PWM excitation (FPE), interior permanent-magnet synchronous motor (IPMSM), indirect flux detection by on-line reactance measurement (INFORM), sensorless.**

I. Introduction

INTERIOR permanent-magnet synchronous motors (IPMSMs) are increasingly used in diverse industrial, household, and automotive applications due to its high-performance characteristics. Many of these applications require the rotor position information to execute the field-oriented control algorithm for a large operating range and good dynamic performance. Hence, a resolver or encoder attached to the shaft of the rotor is usually used to acquire the rotor position information. However, the presence of the mechanical sensor presents several disadvantages of the reduction of reliability, additional cost, and sensitivity to noise and vibration. And the resolver or encoder signal wiring also reduces the reliability of commissioned drive systems. Therefore, various sensorless techniques for IPMSMs control has attracted considerable research over recent years [1]–[26].

Sensorless control techniques can be roughly categories into methods based on the back electromotive force (EMF) model and machine saliency. Methods based on EMF model are widely used due to their simplicity and straightforwardness. They can achieve good performance at middle-high speed, but perform badly in the low and zero speed range where the machine's back-EMF is lost in noise and low measurement resolution [1]–[9]. Saliency-based position estimation solutions are the appropriate way to estimate the rotor position when the motor runs in the zero/low speed. There are different methods based on how they locate the special position of this saliency. A high-frequency injecting-signal method is used to estimate the rotor position of IPMSMs. By injecting a rotating high-frequency signal [9], [10], an alternating high-frequency signal [11], [12], or a high-frequency pulse pattern [13], [14] into the stationary reference frame or estimated synchronous reference frame, the position information can be precisely measured. However, a high-frequency generator and an extra observer for signal processing are required.

A promising approach is the indirect flux detection by on-line reactance measurement (INFORM)-based method, which is very easy in principle and yields excellent results [15]–[18]. Its basic idea is to measure the current response evoked by voltage space vectors applied in different directions. There are many possibilities to apply these space vectors. In its typical implementation, one test vector is injected during the null part of one PWM cycle while an equal and opposite vector is applied to compensate for the voltage distortion caused by the test vector. Three successive cycles are usually spent to generate voltage space vectors applied in different directions. It means that a position sample is built up over three cycles with one di/dt measurement per cycle. This approach may cause unacceptable errors at higher speed range, as well as current ripples, current harmonics and extra switching loss will be increased. In order to reduces the current distortion significantly, a modified INFORM measurement sequence with minimum current deviation and time demand is introduced in [15]. However, a specified and modified pulsewidth-modulation (PWM) switching pattern

Manuscript received March 17, 2017; revised July 1, 2017; accepted August 12, 2017. Date of publication August 21, 2017; date of current version March 5, 2018. This work was supported by the National Natural Science Foundation of China under Grant 61472154. Recommended for publication by Associate Editor Dr. Julia Zhang. *(Corresponding author: Qipeng Tang.)*

The authors are with the Key Laboratory of Electronic Power and Power Transformation, School of Automation, Huazhong University of Science and Technology, Wuhan 430074, China (e-mail: hust_luox@126.com; d201377541@hust.edu.cn; sawyi@mail.hust.edu.cn; 764704982@qq.com; jbxuhust@gmail.com).

Color versions of one or more of the figures in this paper are available online at http://ieeexplore.ieee.org.

Digital Object Identifier 10.1109/TPEL.2017.2743106

is required, which not only increases the difficulty in implementations but also multiplies the switching loss. An excellent technique to inject voltage test vector coupled with zero sequence current derivatives (ZSCD) measurements is adopted for the rotor position estimation [19]–[21]. Although this technique has advantages of high vector control performance and simple estimation process, the neutral point of the motor must be accessible for exciting the zero sequence component, which is not suitable for general industrial application. The normal FPE can also be regarded as voltage space vectors for the rotor position estimation [22]–[26]. Since it is very effective and robust because no extra circuit and injecting signal are required, modifying PWM switching states are necessary for the acquisition of voltage space vectors in different directions, which increases the difficulty in implementations, line current harmonic distortion, as well as switching loss. In view of a standstill or sector switching condition where the duration of the active vector of fundamental PWM excitation (FPE) cannot satisfy the time demand for the resulting current sampling, three compensation techniques are proposed to improve the quality of the position estimation and reduce current distortion [24]. For the little line current ripple, a novel PWM schemes for multi-space-vector PWM is proposed in [25]. In which, six sequences is adopted for zero-/low-speed operation and 24 sequences is used for high-speed operation for the applicability in wide speed range. To reduce the line current harmonic distortion as well as switching loss, an advanced bus-clamped SVPWM technique is presented [26]. Meanwhile, multiple division of active vector time (MDAVT) is introduced to effectively generate voltage space vectors applied in different directions.

Summarizing the available literatures, although these INFORM-based methods have their respective advantages, the problems in the typical INFORM-based method, such as complicated implementation, extra switching loss, estimation errors, or current harmonic distortions, are not solved satisfactorily. In order to effectively solve these problems, a hybrid strategy to combine FPE and additional test vectors is proposed. With the proposed method, voltage space vectors applied in different directions for the rotor position estimation can be obtained from both the active vectors of FPE and additional test vectors in one PWM cycle, which makes the proposed strategy robust and suitable in higher speed or load sudden change conditions. Meanwhile, a new PWM scheme for four-space-vector PWM (FSVPWM) is presented, which sharply simplifies the implementation process as well as does not increase extra switching number of power switching devices. Furthermore, aiming at a standstill or low speed where the amplitude of the object fundamental voltage is so small that it cannot satisfy minimum time demand for the slopes of response currents sampling, a compensation technique is presented. In addition, multiple-point current sampling (MPCS) technology and linear least square fitting method are used to decrease the current sampling disturbance, which improves obviously the accuracy of position estimation. Finally, the experimental results confirm that the proposed strategy can obtain the rotor position accurately and simply.

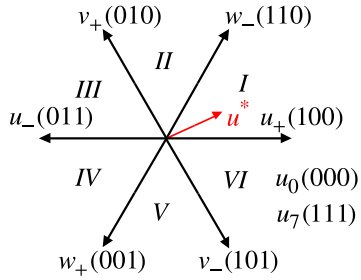

Fig. 1. Definition of space vectors.

II. Typical INFORM-Based Implementation Scheme

The basic model of an IPMSM in the stationary reference frame $\alpha\beta$ is as follows:

$$\begin{bmatrix} v_\alpha \\ v_\beta \end{bmatrix} = \begin{bmatrix} R_s & 0 \\ 0 & R_s \end{bmatrix} \begin{bmatrix} i_\alpha \\ i_\beta \end{bmatrix} + \begin{bmatrix} L_0 + L_1\cos 2\theta & L_1 \sin 2\theta \\ L_1 \sin 2\theta & L_0 - L_1 \cos 2\theta \end{bmatrix} \begin{bmatrix} \frac{di_\alpha}{dt} \\ \frac{di_\beta}{dt} \end{bmatrix} + \omega_r \left(2L_1 \begin{bmatrix} -\sin 2\theta & \cos 2\theta \\ \cos 2\theta & \sin 2\theta \end{bmatrix} \begin{bmatrix} i_\alpha \\ i_\beta \end{bmatrix} + \psi_{pm} \begin{bmatrix} -\sin\theta \\ \cos\theta \end{bmatrix} \right)$$
$$L_0 = \frac{L_d + L_q}{2}, \qquad L_1 = \frac{L_d - L_q}{2} \tag{1}$$

where v_α and v_β are the stator voltages, i_α and i_β are the stator currents in the stationary reference frame $\alpha\beta$, R_s is the motor resistance, and $\psi_{\rm pm}$ is the permanent magnet's flux linkage. L_d, L_q are the direct and quadrature inductance in the rotor-oriented reference frame *dq*. The IPMSM is driven by a three-phase voltage-source inverter. The inverter has eight permissible switching sates: six active states ($u_+ \sim v_-$) and two inactive states (u_0, u_7), as shown in Fig. 1.

The INFORM-based method is a classical rotor position estimation method which utilizes the saliency of the rotor. Its basic idea is to create desired current responses by injecting several test voltage vectors, and the rotor position is calculated from the resulting current slopes.

When the vector u_+ is applied to the machine, the current slope is deduced as

$$\frac{di_a^{(u_+)}}{dt} = I_0 \left[\frac{2}{3} V_{\rm dc} \left(L_0 - L_1 \cos 2\theta \right) - C_{rs} - \frac{1}{3}\omega_r L_1 \left(-6L_0 i_a \sin 2\theta + \sqrt{3}\left(i_b - i_c \right) \times \left(-2L_1 + 2L_0 \cos 2\theta \right) + \psi_{\rm pma} \right) \right] \tag{2}$$

with

$$I_0 = \frac{1}{L_0^2 - L_1^2}, \quad \psi_{\rm pma} = \frac{3\psi_{\rm pm}}{L_1}\left(L_0 - L_1 \right)\cos\theta$$
$$C_{rs} = R_s \left(-L_1 i_a \cos\left(2\theta \right) - \frac{\sqrt{3}}{3} L_1 \left(i_b - i_c \right) \sin\left(2\theta \right) + L_0 i_a \right)$$

where $V_{\rm dc}$ is the bus voltage of the inverter; v_a, v_b, and v_c are the motor terminal voltages; and i_a, i_b, and v_c are the motor phase currents in the stationary reference frame *abc*.

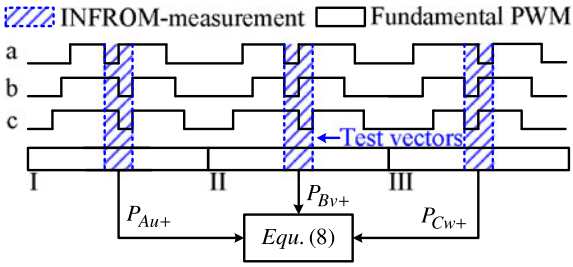

Fig. 2. Typical INFORM-based implementation scheme.

Then, when the inactive vector u_0 is applied to the machine, the current slope is induced as

$$\frac{di_a^{(u_0)}}{dt} = I_0\left[-C_{rs} - \frac{1}{3}\omega_r L_1\left(-6L_0 i_a \sin 2\theta + \sqrt{3}\left(i_b - i_c\right)\right.\right. \times \left.\left.\left(-2L_1 + 2L_0\cos 2\theta\right) + \psi_{\mathrm{pma}}\right)\right]. \tag{3}$$

Note that u_0 can be replaced by u_7, depending on the convenience of their measurement. Under the assumption that three phase currents i_a, i_b, and i_c are consistent during one PWM period, (2) and (3) has

$$P_{Au_+} = \frac{di_a^{(u_+)}}{dt} - \frac{di_a^{(u_0)}}{dt} = \frac{2}{3}I_0 V_{\mathrm{dc}}\left(L_0 - L_1\cos 2\theta\right). \tag{4}$$

Similarly, when other active vectors are applied to the machine, the following expressions can be also obtained:

$$P_{Bv_+} = \frac{di_b^{(v_+)}}{dt} - \frac{di_b^{(u_0)}}{dt} = \frac{2}{3}I_0 V_{\mathrm{dc}}\left(L_0 - L_1\cos\left(2\theta + \frac{2\pi}{3}\right)\right) \tag{5}$$

$$P_{Cw_+} = \frac{di_c^{(w_+)}}{dt} - \frac{di_c^{(u_0)}}{dt} = \frac{2}{3}I_0 V_{\mathrm{dc}}\left(L_0 - L_1\cos\left(2\theta + \frac{4\pi}{3}\right)\right) \tag{6}$$

$$P_{Au_-} = -P_{Au_+}, \quad P_{Bv_-} = -P_{Bv_+}, \quad P_{Cw_-} = -P_{Cw_+}. \tag{7}$$

Finally, using an arctangent function to calculate the rotor position by solving (4), (5), and (6). It is noteworthy that u_+ (v_+, w_+) can be replaced by u_- (v_-, w_-), depending on the convenience of their measurement because the role of the vector u_- (v_-, w_-) for the rotor position estimation is equivalent to that of the vector u_+ (v_+, w_+)

$$\theta = 0.5 * \tan^{-1}\left(\frac{\sqrt{3}\left(-P_{Bv_+} + P_{Cw_+}\right)}{2P_{Au_+} - P_{Bv_+} - P_{Cw_+}}\right). \tag{8}$$

It is obviously observed that the INFORM-based method is effective and independent of any motor parameters in principle. The keystone and difficulty is how to get current responses evoked by test voltage vectors $u_+(u_-)$, $v_+(v_-)$, $w_+(w_-)$ and the inactive vector (u_0 or u_7) simultaneously. Its commonly adopted implementation scheme is shown in Fig. 2. Observed from Fig. 2, test voltage vectors u_+, v_+, and w_+ are inserted only in the null part of three successive PWM cycles, respectively, while equal and opposite vectors u_+, v_+, and w_+ are inserted to counteract their influences on the fundamental-wave control. The rotor position θ can be obtained from the response currents by using (8). However, with the motor speed increasing, the three-cycle acquisition of the rotor position in the typical INFORM-based implementation scheme has large estimation errors because the rotor position cannot be equivalent during three successive PWM cycles, which restricts its application in higher speed or load sudden change conditions. Furthermore, the injection of extra test vectors bring extra switching loss due to the increasing number of power switching devices during one PWM cycle.

TABLE I
APPLIED VOLTAGE VECTORS IN EACH SECTOR

Sector	Existing Active Vectors	Required Test Vectors
I	u_+, w_-	v_+, v_-
II	v_+, w_-	u_+, u_-
III	v_+, u_-	w_+, w_-
IV	w_+, u_-	v_+, v_-
V	w_+, v_-	u_+, u_-
VI	u_+, v_-,	w_+, w_-

III. Proposed Sensorless Control Strategy

Although the INFORM-based method has advantages of simple physical principle and independence of any motor parameters, its typical implementation is usually complicated and the acquisition of the rotor position needs to cost three PWM cycles. Differing from the typical INFORM-based method, a hybrid sensorless control strategy to combine FPE and additional test vectors is proposed, which brings improvement in implementation, switching loss, real-time acquisition of rotor position estimation.

A. Proposed Sensorless Control Strategy

As obviously observed from Fig. 2, test voltage vectors are only inserted in the null part of one PWM cycle while the existing active vectors of FPE are discarded, which leads to the low effective time slice used for the acquisition of the rotor position information during one PWM cycle. That's the reason why it needs to cost three successive PWM cycles to estimate the rotor position. However, it's obviously found that the active vectors of FPE are parts of required test voltage vectors. If the active vectors of FPE can be used for the acquisition of the rotor position information, the effective time slice for the acquisition of the rotor position information can be dramatically expanded and the rotor position estimation is expected to be achieved during one PWM cycle. Based on this idea, a hybrid strategy to combine FPE and additional test vectors is proposed for IPMSM sensorless control. With the proposed strategy, additional test voltage vectors are determined based on two active vectors of FPE rather than a certain fixed sequence of test vectors in the typical INFORM-based implementation scheme. Taking the example for sector I, as two active vectors of FPE are u_+ and w_-, the required test voltage vector is selected as vector v_+ by reference to (5)–(8). Meanwhile, the equal and opposite vector v_- is inserted to counteract their influences on the fundamental-wave

TABLE II
CALCULATION EXPRESSION OF ROTOR POSITION

Sector	The Estimated Rotor Position Expression θ
I, II	$0.5 * \tan^{-1}\left(\frac{\sqrt{3}(-P_{Bv_+} - P_{Cw_-})}{2P_{Au_+} - P_{Bv_+} + P_{Cw_-}}\right)$
III, IV	$0.5 * \tan^{-1}\left(\frac{\sqrt{3}(-P_{Bv_+} + P_{Cw_+})}{-2P_{Au_-} - P_{Bv_+} - P_{Cw_+}}\right)$
V, VI	$0.5 * \tan^{-1}\left(\frac{\sqrt{3}(P_{Bv_-} + P_{Cw_+})}{2P_{Au_+} + P_{Bv_-} - P_{Cw_+}}\right)$

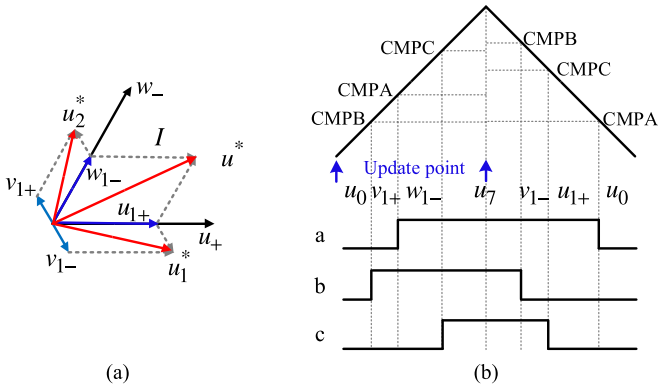

Fig. 3. FSVPWM. (a) Equivalent grouping of four voltage vectors. (b) Schematic diagram of PWM counter update.

control for the little current jitter. Table I gives the corresponding applied voltage vectors in each sector. It is worth noting that the acquisition of the current deviation evoked by u_0 (u_7) is not described in the following sections because the inactive vector u_0 (u_7) generally exists in every PWM cycle.

According to the derivation of (2)–(8), the calculation expression of the rotor position can be gotten in each sector, as shown in Table II.

With the proposed method, there are still four active vectors (described as in Table I) that are required to be generated in each PWM cycle. In order to generate them simply and effectively, an FSVPWM implementation scheme is presented. The proposed implementation scheme has two steps: first, the four active vectors are divided into two groups, and then, one of two groups is generated in the rising edge and another is produced in fall edge by means of PWM counter double update mechanism of microcontroller. Taking the example for sector I, first, the four active vectors (u_{1+}, w_{1-}, v_{1+}, and v_{1-}, as described in Table I) are divided into two groups: w_{1-} and v_{1+} are as a group to generate u_2* and u_{1-} and v_{1-} are as another group to generate u_1*, as shown in Fig. 3(a). Namely, the reference voltage u^* is equivalent synthesized from u_1^* and u_2^*. The schematic diagram of PWM counter update is described in Fig. 3(b). In which, CMPA, CMPB, and CMPC are the count-compare registers of the microcontroller. u_2^* is produced in the rising edge of the PWM counter and updated in the peak of the PWM counter. u_1^* is produced in the fall edge of PWM and updated in the valley of PWM. Finally, according to the description of Table II, the rotor position θ can be obtained from the resulting current deviations. The same process can be implemented in other sectors.

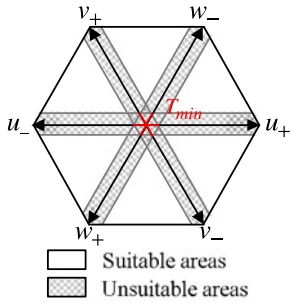

Fig. 4. Suitable areas of proposed method.

With the proposed sensorless control strategy, the rotor position θ is obtained from the resulting current slopes of both FPE and additional test vectors in one PWM cycle rather than three successive PWM cycles of the typical INFORM-based implementation scheme. The one-cycle acquisition of the rotor position not only expands the applicable speed range but also improves the dynamic property of control system. Furthermore, a new FSVPWM scheme is presented, which sharply simplifies the implementation process as well as effectively reduces the switching loss.

B. *Effective Active Zone*

According the earlier analysis, the resulting current slopes evoked by four required active vectors have to be measured in the proposed method. It implies a minimum duration $T_{\min}$ of required switching vector is necessary for the power electronics as well as for the current sensor outputs after the switching transients. In the proposed strategy, the duration of test voltage vectors can be artificially set to satisfy the minimum duration $T_{\min}$. But the duration of the active vectors of FPE are changing with the reference voltage of the fundamental-wave excitation. There are some specific points of operation where one or even either of two active vectors of FPE may not satisfy the minimum duration $T_{\min}$. Especially at low or zero fundamental frequency, due to the low modulation, they may be omitted due to inverter blanking time. But also at high-modulation indices in the areas where the reference voltage changes between two neighboring sectors and passes one of the six possible active switching vectors there is only one active switching vectors of appropriate length. The hatched areas where the proposed sensorless control strategy is not suitable are depicted in Fig. 4.

In order to reduce these unsuitable areas descried in the hatched areas of Fig. 4, the duration time of four active vectors in the proposed method can be adjusted to not only counteract their influences on the fundamental-wave control but also satisfy the minimum duration $T_{\min}$ when the reference voltage changes between two neighboring sectors at high-modulation indices. Similarly, taking the example for sector I, according to the proposed method in Section A, the four voltage vectors are u_{1+}, w_{1-}, v_{1+} and v_{1-} (as shown in Table I) and their duration are t_1, t_2, $T_{\min}$, $T_{\min}$, respectively, described with blue arrows in Fig. 5. When the reference voltage u^* changes between two neighboring sectors at high-modulation indices, one of t_1 and

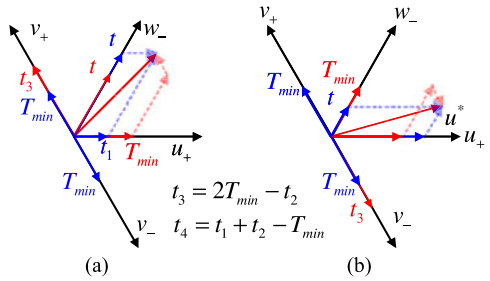

Fig. 5. Description of improved proposed strategy in the sector I.

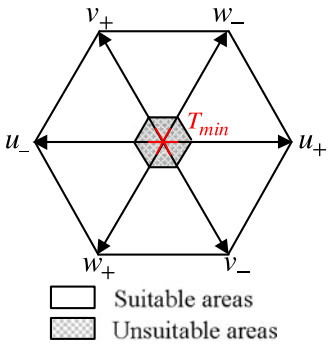

Fig. 6. Effective active areas with improved method.

t_2 is smaller than $T_{\min}$. First, suppose t_1 is smaller than $T_{\min}$ and t_2 is longer than $T_{\min}$ in Fig. 5(a). In order to satisfy the effective current sampling time for the rotor position estimation, expand the duration time of u_{1+} to $T_{\min}$ while the duration time of w_{1-}, v_{1+}, and v_1 are adjusted as t_4, t_3, $T_{\min}$, respectively, described with red arrows in Fig. 5(a).

The duration time t_4, t_3 must be longer than $T_{\min}$. The expressions are presented as

$$\begin{cases} t_2 \le T_{\min} \\ t_1 + t_2 \ge 2T_{\min} \end{cases}. \tag{9}$$

The same result is suitable in other case that t_2 is smaller than $T_{\min}$ and t_1 is longer than $T_{\min}$, as described in Fig. 5(b). Thus, the required applicable condition can be represented as

$$\begin{cases} t_1 \text{ or } t_2 \le T_{\min} \\ t_1 + t_2 \ge 2T_{\min} \end{cases}. \tag{10}$$

By adjusting the duration time of four required active vectors, the hatched areas where the proposed sensorless control strategy is not suitable are as depicted in Fig. 6. In contrast to Fig. 4, it can be obviously found that the unsuitable area is reduced dramatically.

C. Compensation Solution

For the rest unsuitable hatched areas in Fig. 6, a compensation implementation solution that use two successive PWM cycles to estimate the rotor position is presented in this section. In the first PWM cycle, expand the duration of two fundamental active vectors to the minimum duration $T_{\min}$ to satisfy the effective current sampling for the rotor position estimation while

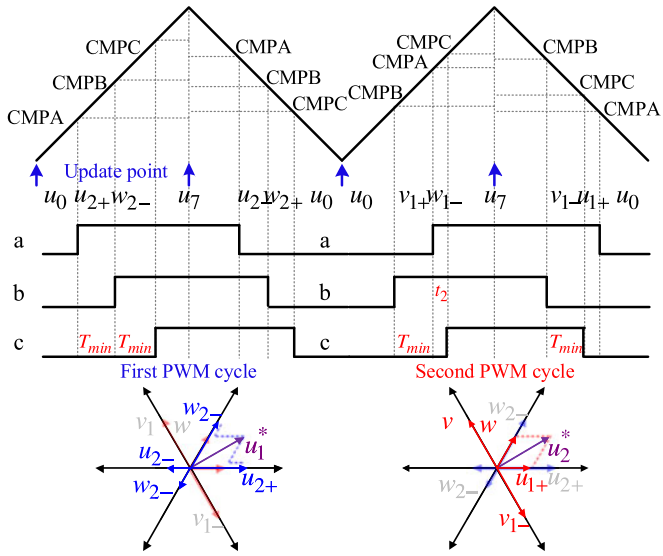

Fig. 7. Schematic diagram of PWM counter update with same sector of SVPWM during two successive PWM cycles.

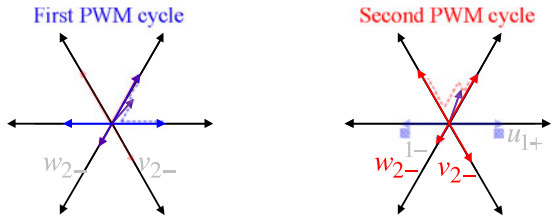

Fig. 8. Schematic diagram of PWM counter update with different sector of SVPWM during two successive PWM cycles.

the opposite vectors are injected to ensure that the synthesizing vector is equal to the reference voltage. The resulting current deviations evoked by these two fundamental active vectors are sampled and recorded. Then, in the second PWM cycle, there are two steps. First, get the new voltage reference u_2* and sector of SVPWM. Second, determine if the sector in the second PWM cycle and the sector in the first PWM cycle are the same or different. If the same, additional test vectors with the duration time $T_{\min}$ are selected and injected in the second PWM cycle according to Table I regardless of the duration of fundamental active vectors. And only the slope of the response current evoked by the additional test vector is sampled and recorded. If different, expand one of two fundamental active vectors in the second PWM cycle that is different from two fundamental active vectors in the first PWM cycle to the minimum duration $T_{\min}$ for the effective current sampling. Only the slope of the response current evoked by the expanded fundamental active vector in the second PWM cycle is sampled and recorded. Finally, the rotor position is gotten during two successive PWM cycles. Similarly, taking the example for sector I, the reference value $u*$ lied in hatched areas of Fig. 6 is adjusted by applying two fundamental active vectors u_{1+}, w_{1-} and their duration times are t_1 and t_2, respectively. According the analysis given in Section III-B, relations between t_1 and t_2 can be presented

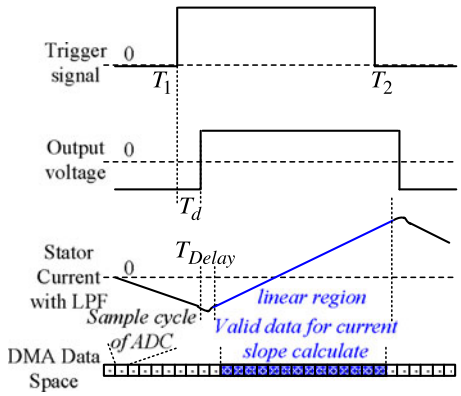

Fig. 9. Process of current sampling.

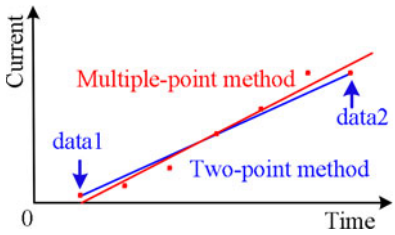

Fig. 10. Comparison of current slope with MPCS and conventional two-point sampling technique.

as follows:

$$\begin{cases} t_1 \text{ or } t_2 \le T_{\min} \\ t_1 + t_2 < 2T_{\min} \end{cases} \text{or} \quad \begin{cases} t_1 < T_{\min} \\ t_2 < T_{\min} \end{cases}. \tag{11}$$

Might as well choose the case that both t_1 and t_2 are smaller than $T_{\min}$ to be analyzed. The result is also applicable in another case. In the first PWM cycle, expand two fundamental active vectors u_{1+} and w_{1-} to u_{2+} and w_{2-} while the opposite vectors u_{2-} and w_{2+} are injected to ensure the synthesizing vector is equal to u_1^*. Their duration times of u_{2+}, w_{2-}, u_{2-}, and w_{2+} are $T_{\min}$, $T_{\min}$, $T_{\min} - t_1$, and $T_{\min} - t_2$, respectively. The resulting current deviations evoked by u_{2+} and w_{2-} are sampled and recorded. And then, in the second PWM cycle, there are two steps. First, get the new voltage reference u_2* and sector of SVPWM. Second, determine if the sector in the second PWM cycle and the sector in the first PWM cycle are the same or different. If the same, four required vectors composed of two fundamental active vectors u_{1+} and w_{1-} and two additional test voltage vectors v_{1+} and v_{1-} are applied. Their duration times are t_1, t_2, $T_{\min}$ and $T_{\min}$, respectively, as shown in Fig. 7. Only the slope of the response current evoked by v_{1+} is sampled and recorded. If different, expand v_{1+} or v_{1-} in the second PWM cycle to the minimum duration $T_{\min}$ while the opposite vectors v_{2-} or v_{2+} is injected to ensure the synthesizing vector is equal to $u*$, as shown in Fig. 8. Only the slope of the response current evoked by v_{1+} or v_{1-} in the second PWM cycle is sampled and recorded. Finally, according to the description of Table II, the rotor position is calculated during two successive PWM cycles.

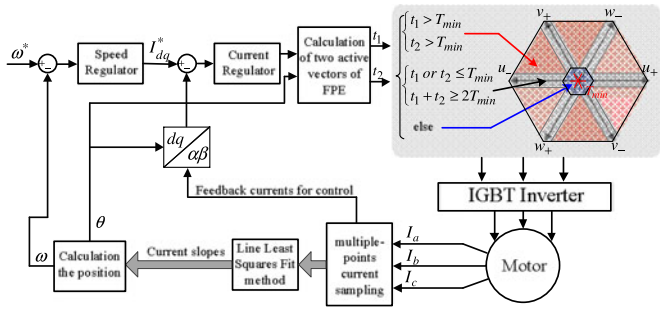

Fig. 11. Overall block diagram of proposed sensorless control strategy.

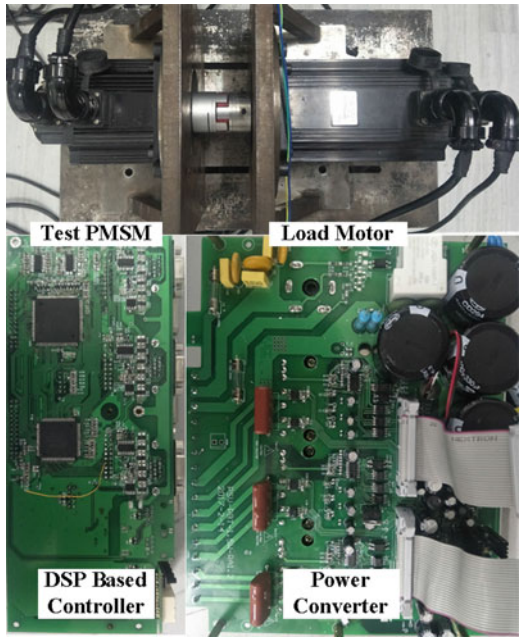

Fig. 12. Experimental setup used to test proposed methods.

D. Acquisition of Current Slope

In the earlier proposed method, the rotor position information is extracted directly from the stator current slopes. However, in the practical application, the selection of the minimum sampling time $T_{\min}$ is very important for the fundamental voltage limitation. And $T_{\min}$ is selected for the accurate sampling current, which is usually determined by the applicable hardware platform, such as hardware delay, sampling errors, random disturbance and dead zone effects of inverter. In order to improve current measurement precision, the MPCS technique based on direct memory access (DMA) module of microcontroller and line least squares fit (LLSF) algorithm are used. With the MPCS technique, the resulting stator currents are consecutively sampled every one AD sampling cycle of microprocessor while consecutively stored in the access memory by using DMA module. Then, the optimal current slope can be obtained by using LLST method to process these successive sampled currents.

Fig. 9 shows the sampling process of one response current. The "linear region" is the only effective sampling region where the data is valid and accurate for current slope calculation. T_1 and T_2 are the start time and end time, respectively. Since the

TABLE III
MOTOR PARAMETERS

Parameter	IPMSM
Rated power	1.8 kW
Rated speed	3000 r/min
Rated current	7.5 A
Rate torque	1.0 N·m/A
Phase resistance	0.9 Ω
d-/*q*-axis inductance	2.5 mH/4.8 mH
Pole numbers	8
Rated voltage	220 V
DC-link voltage	311 V

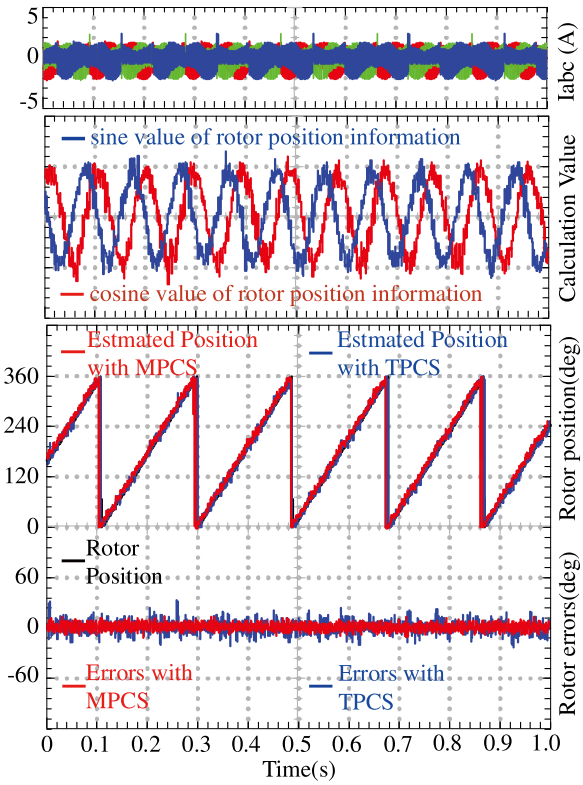

Fig. 13. Contrast experiments of MPCS and TPCS with proposed sensorless control strategy.

actual output voltage always lags behind the control signal a dead time T_d, and the measured current is always behind the actual response current with a delay time T_{Delay} due to the hardware sampling delay, the linear region can be described as

$$\text{Effective region} \in (T_1 - T_d - T_{\text{Delay}}, T_2 + T_d) \tag{12}$$

where T_1, T_2, T_d, and T_{Delay} can be known easily. According to the selected linear region, the continuously sampling data of the response current can be directly read from the DMA's storage space. These current sampling points can be marked as (t_i, C_i), where $i \in (1, N)$, t_i and C_i are the sampling time and corresponding current sampling value, respectively. N is the total sampling number. Then, by applying LLSF method to process these sampling points, the optimal current slope K can

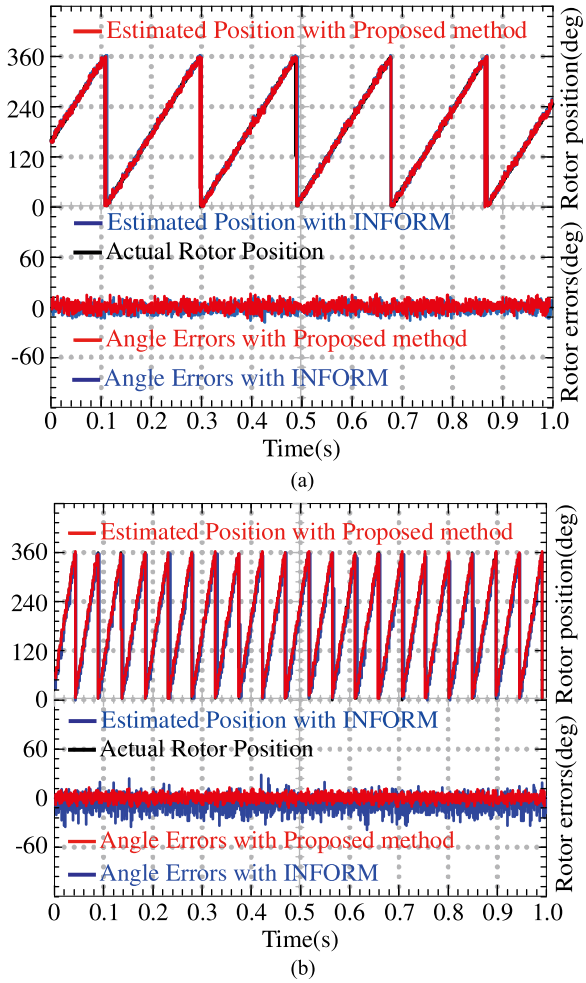

Fig. 14. Comparison of angle errors with different methods. (a) With amplitude 75 r/min; (b) with amplitude 300 r/min.

be obtained, as

$$K = \frac{N\sum_{i=1}^{N} t_i C_i - \sum_{i=1}^{N} t_i \cdot \sum_{i=1}^{N} C_i}{N\sum_{i=1}^{N} {t_i}^2 - \left(\sum_{i=1}^{N} t_i\right)^2}. \tag{13}$$

Fig. 10 shows the comparison of the acquisition of the current slope with the MPCS technique and the conventional two-point sampling technique. Obviously, with this MPCS method, the current sampling errors induced by hardware delay, sampling errors, random disturbances can be drastically reduced and the current slope can be measured more effectively and accurately.

IV. EXPERIMENTAL RESULTS

In this section, the effectiveness of the proposed sensorless control hybrid strategy based on FSVPWM is tested experimentally. The total block diagram of the implemented drive system is shown in Fig. 11. And the system setup for experimental testing is shown in Fig. 12. The proposed hybrid strategy is implemented with ADSP-CM408. Two internal 16-b A/D converters with 0.5-μs conversion time are used to improve the precision of

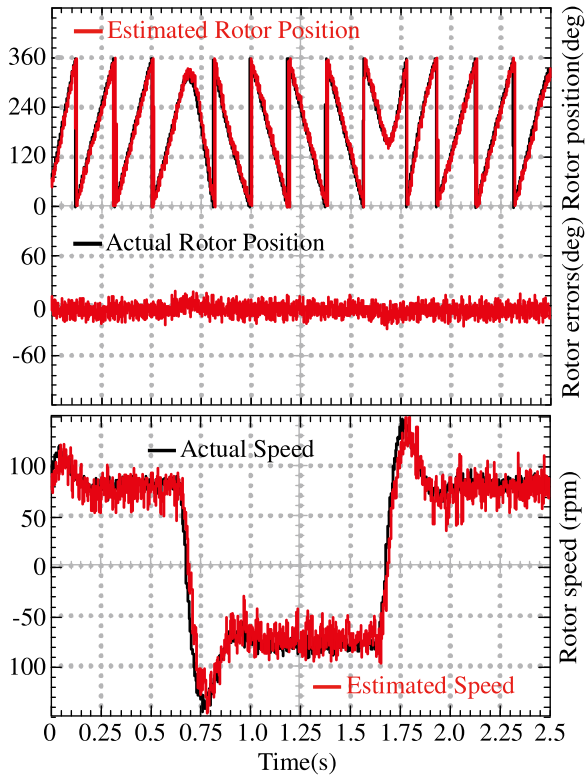

Fig. 15. Following performance under step speed with amplitude 75 r/min.

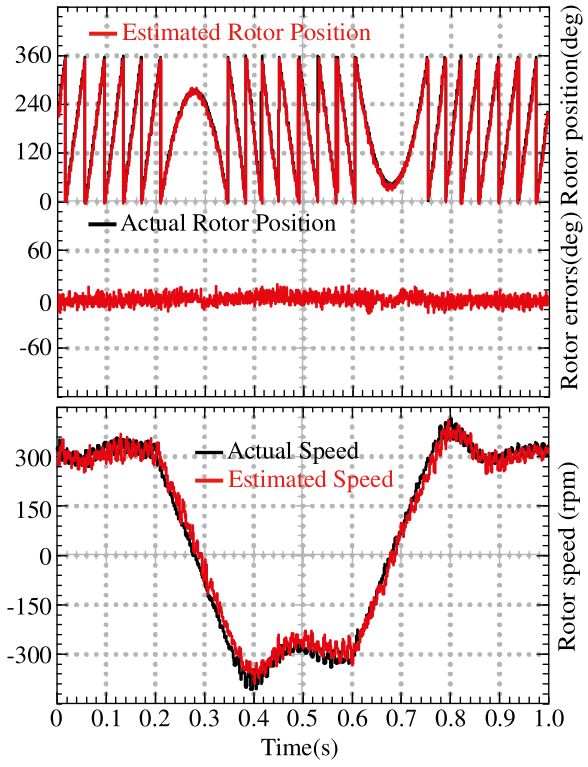

Fig. 16. Following performance under step speed with amplitude 300 r/min.

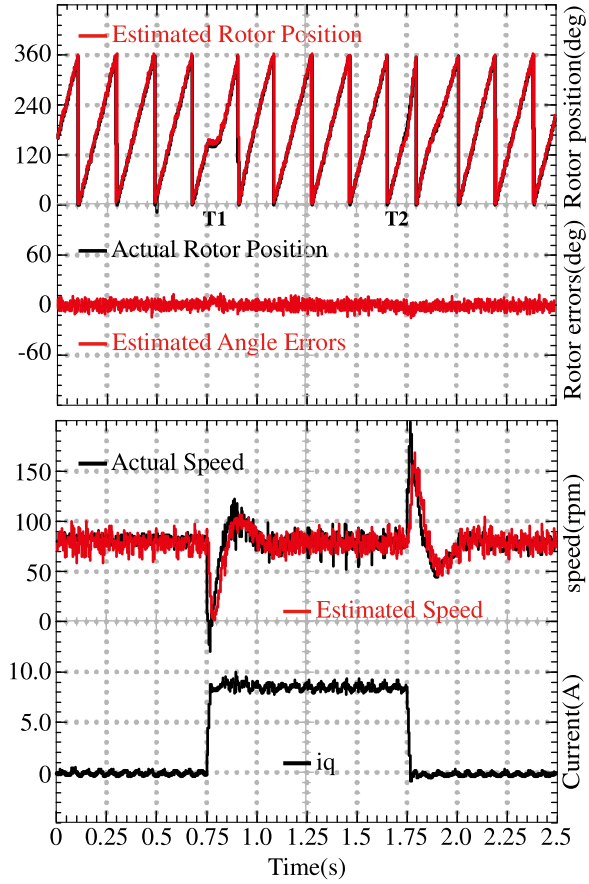

Fig. 17. Dynamic performance under step full load at 75 r/min.

current-ripple measurement. The PWM cycle of the drive is set to 250 μs, the dead time T_d is set to 2.5 μs and the whole delay of hardware processing circuits is about 10 μs by measurement. Because fifteen current sampling points are used, the whole sampling time is 7.5 μs. Actually, for the accurate sampling currents, the larger minimum duration $T_{\min}$ is better. However, the larger minimum duration $T_{\min}$ not only brings the bigger current jitters but also limits the maximum speed and load when the PWM frequency of the drive is set. Thus, a compromise is necessary for the selection of the minimum duration $T_{\min}$. After the comprehensive consideration, the minimum duration $T_{\min}$ is set as 20 μs in this paper. The specification and parameters of the testing PMSM is listed in Table III. And another motor is used to provide the load torque. An incremental encode is equipped to provide the actual rotor position. It is noted that all the experimental results are presented in oscilloscope by using D/A modules.

The proposed sensorless control strategy based on the proposed MPCS technique and the conventional two-point current sampling (TPCS) method are implemented in Fig. 13. The reference speed is set as 75 r/min. Fig. 13(a) shows the relationships of sine and cosine function to the electrical-rotor position of the motor θ and three-phase stator currents. Then the rotor position can be easily calculated by using an arctangent function. As the noise always exists in the hardware system, the MPCS technique

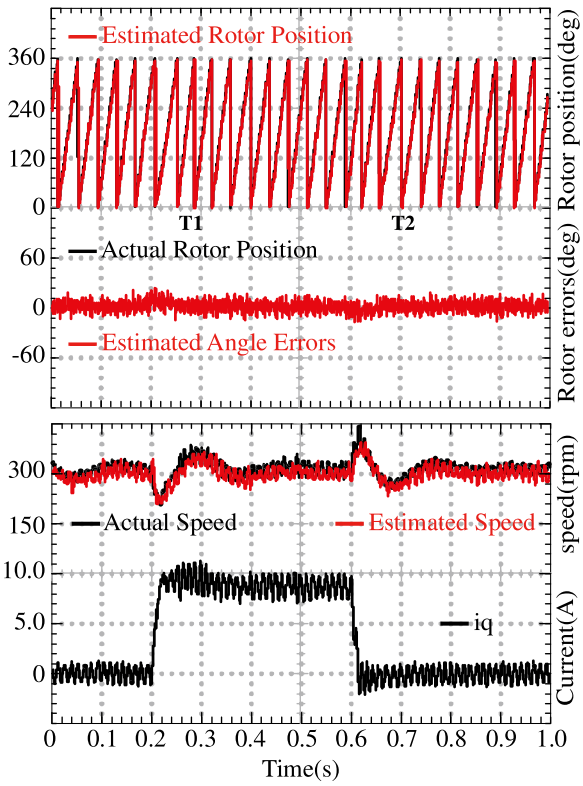

Fig. 18. Dynamic performance under step full load at 300 r/min.

is used to reduce the sampling current noise and improve the signal-to-noise ratio (SNR). The curves of their rotor position estimation and their corresponding position estimation errors relative to the actual rotor position provided by the incremental encode are presented in different colors, respectively. It can be observed that the rotor position estimation based on the proposed MPCS technique can match the actual rotor position well, and the errors are within plus and minus 10 electrical degrees.

To show the superiority of the proposed method over the typical INFORM method, some comparative experiments are carried out. Fig. 14(a) shows the comparative results of rotor position estimation when the speed is set as 75 r/min. It can be obviously observed that similar results are gotten with these two methods. The reason is that the rotor position has little changes during one, two, or three PWM periods at low speed. Fig. 14(b) gives the experimental results in higher speed. Considering the voltage limitation, the speed is set as 300 r/min. It can be observe that the estimated position with the typical INFORM method has greater jitters and errors than that with the proposed method.

To show the following performance of the proposed method, experimental results of speed reversal under no-load condition are described in Figs. 15 and 16. The machine is accelerated from standstill to 75 r/min; the speed is then reversed to -75 r/min, and then the motor goes back to 75 r/min. The estimated rotor position, the actual rotor position, the estimation errors, the corresponding estimated speed, and the actual speed curves are presented, respectively, as described in Fig. 15. The same experiments are carried out when the speed is 300 r/min and reversal. The results are described in Fig. 16. It can be seen that the steady-state performance and the dynamic performance are excellent with the proposed sensorless control strategy.

Figs. 17 and 18 show the dynamic performance of the proposed method when the load step changes from no load to full load at 75 and 300 r/min. At T1, the full load is applied in the machine, and then released at T2. Since little fluctuations appear on the position estimation waveform at these instants, position estimation errors change back to the normal level after a while. The estimated rotor position, the actual rotor position, the estimation errors, the corresponding speed and load current curves are described, respectively, as described in Fig. 17. The same experiments are carried out when the speed sets 300 r/min. The results are shown in Fig. 18. The experimental results indicate the proposed sensorless control strategy has certain robustness in the load sudden conditions.

V. Conclusion

The typical INFORM-based methodology has increasingly attracted researchers' interest for IPMSM sensorless control due to its simple physical principle. Differing from the typical INFORM-based methodology that the rotor position is calculated and updated every three successive PWM cycles, a hybrid strategy to combine FPE and additional test vectors is proposed. With the proposed strategy, the selection of additional test vectors is based on the duration and direction of two fundamental active vectors and the rotor position information is obtained from both the resulting current deviations of FPE and additional test vectors in one PWM cycle. To simplify the implementation process, a new PWM scheme for FSVPWM is presented. Aiming at narrow vectors induced by the small amplitude of the object fundamental voltage where the duration of active vectors cannot satisfy the minimum time demand for the response currents sampling, a compensation technique is presented to improve the quality of the position estimation and reduce current distortion. In addition, the MPCS technique and linear least square fitting method are used to decrease the current sampling disturbance, which can improve obviously the accuracy of the rotor position estimation. Finally, the experimental results confirm that the proposed strategy can obtain the rotor position accurately and simply.

References

[1] Y. Zhao, Z. Zhang, W. Qiao, and L. Wu, "An extended flux model-based rotor position estimator for sensorless control of salient-pole permanent-magnet synchronous machines," *IEEE Trans. Power Electron.*, vol. 30, no. 8, pp. 4412–4422, Aug. 2015.

[2] J. B. Liu, T. A. Nondahl, P. B. Schmidt, S. Royak, and M. Habaugh, "Rotor position estimation for synchronous machines based on equivalent EMF," *IEEE Trans. Ind. Appl.*, vol. 47, no. 3, pp. 1310–1318, May/Jun. 2011.

[3] K. Q. Nguyen, T. H. Nguyen, and Q. P. Ha, "FPGA-based sensorless PMSM speed control using reduced-order extended Kalman filters," *IEEE Trans. Ind. Electron.*, vol. 61, no. 12, pp. 6574–6582, Dec. 2014.

[4] T. Bernardes, V. F. Montagner, H. A. Grundling, and H. Pinheiro, "Discrete-time sliding mode observer for sensorless vector control of permanent magnet synchronous machine," *IEEE Trans. Ind. Electron.*, vol. 61, no. 4, pp. 1679–1691, Apr. 2014.

[5] H. A. A. Awan, T. Tuovinen, S. E. Saarakkala, and M. Hinkkanen, "Discrete-time observer design for sensorless synchronous motor drives," *IEEE Trans. Ind. Appl.*, vol. 52, no. 5, pp. 3968–3979, Sep./Oct. 2016.

[6] G. Haines and N. Ertugrul, "Wide speed range sensorless operation of brushless permanent-magnet motor using flux linkage increment," *IEEE Trans. Power Electron.*, vol. 63, no. 7, pp. 4052–4060, Jul. 2016.
[7] L. Rovere, A. Formentini, A. Gaeta, P. Zanchetta, and M. Marchesoni, "Sensorless finite-control set model predictive control for IPMSM drives," *IEEE Trans. Ind. Electron.*, vol. 63, no. 9, pp. 5921–5931, Sep. 2016.
[8] M. S. Rafaq, F. Mwasilu, J. Kim, H. H. Choi, and J. W. Jung, "Online parameter identification for model-based sensorless control of interior permanent magnet synchronous machine," *IEEE Trans. Power Electron.*, vol. 32, no. 6, pp. 4631–4643, Jul. 2017.
[9] M. Seilmeier and B. Piepenbreier, "Sensorless control of PMSM for the whole speed range using two-degree-of-freedom current control and HF test current injection for low-speed range," *IEEE Trans. Power Electron.*, vol. 30, no. 8, pp. 4394–4402, Aug. 2015.
[10] Z. Chen, J. B. Gao, F. X. Wang, Z. X. Ma, Z. B. Zhang, and R. Kennel, "Sensorless control for SPMSM with concentrated windings using multisignal injection method," *IEEE Trans. Ind. Electron.*, vol. 61, no. 12, pp. 6624–6634, Dec. 2014.
[11] P. L. Xu and Z. Q. Zhu, "Novel carrier signal injection method using zero-sequence voltage for sensorless control of PMSM drives," *IEEE Trans. Ind. Electron.*, vol. 63, no. 4, pp. 2053–2061, Apr. 2016.
[12] D. Kim, Y. C. Kwon, S. K. Sul, J. H. Kim, and R. S. Yu, "Suppression of injection voltage disturbance for high-frequency square-wave injection sensorless drive with regulation of induced high-frequency current ripple," *IEEE Trans. Ind. Appl.*, vol. 52, no. 1, pp. 302–312, Jan./Feb. 2016.
[13] R. Ni, D. Xu, F. Blaabjerg, K. Lu, G. Wang, and G. Zhang, "Square-wave voltage injection algorithm for PMSM position sensorless control with high robustness to voltage errors," *IEEE Trans. Power Electron.*, vol. 32, no. 7, pp. 5425–5437, Jul. 2017.
[14] S. C. Yang and Y. L. Hua, "Full speed region drive of permanent-magnet machine combining saliency-based and back-EMF-based drive," *IEEE Trans. Ind. Electron.*, vol. 64, no. 2, pp. 1092–1101, Feb. 2017.
[15] E. Robeischl and M. Schroedl, "Optimized INFORM measurement sequence for sensorless PM synchronous motor drives with respect to minimum current distortion," *IEEE Trans. Ind. Appl.*, vol. 40, no. 2, pp. 591–598, Mar./Apr. 2004.
[16] J. L. Shi, T. H. Liu, and Y. C. Chang, "Position control of an interior permanent-magnet synchronous motor without using a shaft position sensor," *IEEE Trans. Ind. Electron.*, vol. 54, no. 4, pp. 1989–2000, Jun. 2007.
[17] M. A. Vogelsberger, S. Grubic, T. G. Habetler, and T. M. Wolbank, "Using PWM-induced transient excitation and advanced signal processing for zero-speed sensorless control of AC machine," *IEEE Trans. Ind. Electron.*, vol. 57, no. 1, pp. 365–374, Jan. 2010.
[18] G. Xie, K. Lu, S. K. Dwivedi, and J. R. Rosholm, "Improved INFORM method by minimizing the inverter nonlinear voltage error effects" in *Proc. Electr. Mach. Des. Control Diagnosis,* Torino, Italy, 2015, pp. 188–194.
[19] C. S. Staines, C. Caruana, G. M. Asher, and M. Sumner, "Sensorless control of induction machine at zero and low frequency using zero sequence currents," *IEEE Trans. Ind. Electron.*, vol. 53, no. 1, pp. 195–206, Jun. 2006.
[20] R. Leidhold, "Position sensorless control of PM synchronous motors based on zero-sequence carrier injection," *IEEE Trans. Ind. Electron.*, vol. 58, no. 12, pp. 5371–5379, Dec. 2011.
[21] H. Zhan, Z. Q. Zhu, and M. Odavic, "Nonparametric sensorless drive method for open-winding PMSM based on zero-sequence back EMF with circulating current suppression," *IEEE Trans. Power Electron.*, vol. 32, no. 5, pp. 3808–3817, May 2017.
[22] Q. Gao, G. M. Asher, M. Sumner, and P. Makys, "Position estimation of AC machine over a wide frequency range based on space vector PWM excitation," *IEEE Trans. Ind. Appl.*, vol. 43, no. 4, pp. 1001–1011, Jul./Aug. 2007.
[23] S. K. Tseng, T. H. Liu, and J. L. Chen, "Implementation of a sensorless interior permanent magnet synchronous drive based on current deviations of pulse-width modulation switching," *IET Electr. Power Appl.*, vol. 9, no. 2, pp. 95–106, Feb. 2015.
[24] Y. Hua, M. Sumner, G. Asher, Q. Gao, and K. Saleh, "Improved sensorless control of a permanent magnet machine using fundamental pulse width modulation excitation," *IET Electr. Power Appl.*, vol. 5, no. 4, pp. 359–370, Apr. 2011.
[25] M. Gu, S. Ogasaware, and M. Takemoto, "Novel PWM schemes with multi SVPWM of sensorless IPMSM drives for reducing current ripple," *IEEE Trans. Power Electron.*, vol. 31, no. 9, pp. 6461–6475, Sep. 2016.
[26] J. Biswas, M. D. Nair, V. Gopinath, and M. Barai, "An optimized hybrid SVPWM strategy based on multiple division of active vector time (MDAVT)," *IEEE Trans. Power Electron.*, vol. 32, no. 6, pp. 4607–4618, Jun. 2017.

Xin Luo was born in Henan Province, China, in 1986. He received the B.S., M.S., and Ph.D. degrees from the Department of Control Science and Engineering, Huazhong University of Science and Technology (HUST), Wuhan, China, in 2007, 2010, and 2015, respectively.

His current research interests include PMSM drive system, intelligent control, and power conversion circuits.

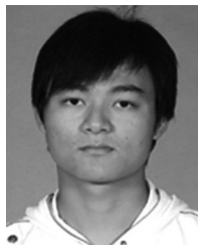

Qipeng Tang (M'17) was born in Jiangxi Province, China, in 1991. He received the B.S. degree in 2013 from the Department of Control Science and Engineering, Huazhong University of Science and Technology (HUST), Wuhan, China, where he is currently working toward the Ph.D. degree at the School of Automation.

His current research interests include power electronics, high-performance ac motor drives, and sensorless control for electrical drives.

Anwen Shen received the B.S. and M.S. degrees from Zhejiang University, Zhejiang, China, in 1991 and 1994, respectively, and the Ph.D. degree from the Huazhong University of Science and Technology (HUST), Wuhan, China, in 1997, all in automation.

In 1997, he joined the Department of Control Science and Engineering, HUST, where he is currently a Professor in the School of Automation. He is a holder of more than ten patents, and several of them have been commercialized. His current research interests include advanced motion control, power electronic application, motor drives, electrical vehicles, and intelligent control.

Hanlin Shen was born in Jiangsu Province, China, in 1990. He received the B.S. degree from the School of Electrical and Information Engineering, Wuhan Institute of Technology (WIT), Wuhan, China, in 2013. He is currently working toward the Ph.D. degree at the School of Automation, Huazhong University of Science and Technology (HUST), Wuhan.

His current research interests include power electronics, high-performance PMSM drives, and intelligent control.

Jinbang Xu was born in Hubei Province, China, in 1973. He received the Ph.D. degree in control science and engineering from the Department of Control Science and Engineering, Huazhong University of Science and Technology (HUST), Wuhan, China, in 2004.

He is currently a professional at the School of Automation, HUST. His current research interests include power electronics, intelligent control, and bioinformatics processing.